Title

Role of Organic Coatings in Regulating N_2O_5 Reactive Uptake to Sea Spray Aerosol

Journal

The Journal of Physical Chemistry A, 119(48)

ISSN

1089-5639 1520-5215

Authors

Ryder, Olivia S
Campbell, Nicole R
Morris, Holly
et al.

Publication Date

2015-12-03

DOI

10.1021/acs.jpca.5b08892

Peer reviewed

On the Role of Organic Coatings in Regulating N_2O_5 Reactive Uptake to Sea Spray Aerosol

Olivia S. Ryder[1], Nicole R. Campbell[1], Holly Morris[2], Sara Forestieri,[3] Matthew J. Ruppel[1], Christopher Cappa[3], Alexei Tivanski[2], Kimberly Prather[1,4] and Timothy H. Bertram[1,5]

[1]*Department of Chemistry and Biochemistry, University of California, San Diego, California, USA*

[2] *Department of Chemistry, University of Iowa, Iowa City, Iowa, USA*

[3] *Department of Civil and Environmental Engineering, University of California, Davis, California, USA*

[4] *Scripps Institution of Oceanography, San Diego, California, USA*

[5]*Now at: Department of Chemistry, University of Wisconsin, Madison, USA*

[*]*Corresponding author. E-mail: *timothy.bertram@wisc.edu*

1. Abstract

Previous laboratory measurements and field observations have suggested that the reactive uptake of N_2O_5 to sea spray aerosol particles is a complex function of particle chemical composition and phase, where surface active organics can suppress the reactive uptake by up to a factor of 60. To date, there are no direct studies of the reactive uptake of N_2O_5 to nascent sea spray aerosol that permit assessment of the role that organic molecules present in sea spray aerosol (SSA) may play in suppressing or enhancing N_2O_5 uptake kinetics. In this study, SSA was generated from ambient seawater and artificial seawater matrices using a Marine Aerosol Reference Tank (MART), capable of producing nascent SSA representative of ambient conditions. The reactive uptake coefficient of N_2O_5 ($\gamma(N_2O_5)$) on nascent SSA was determined using an entrained aerosol flow reactor coupled to a chemical ionization mass spectrometer for measurement of surface area dependent heterogeneous loss rates. Population averaged measurements of $\gamma(N_2O_5)$ for SSA generated from salt water sequentially doped with representative organic molecular mimics, or from ambient seawater, do not deviate statistically from that observed for sodium chloride ($\gamma(N_2O_5)_{NaCl}$ = 0.01-0.03) for relative humidity (RH) ranging between 50-65%. The results are consistent with measurements made under clean marine conditions at the Scripps Institution of Oceanography Pier and those conducted on nascent SSA generated in the marine aerosol reference tank. The results presented here suggest that organic films present on nascent SSA (at RH greater than 50%) likely do not significantly limit N_2O_5 reactive uptake.

2. Introduction

Heterogeneous reactions play a controlling role in both setting the atmospheric lifetime of aerosol particles and catalyzing the production and loss of trace gases in the atmosphere.[1,2] Few heterogeneous reactions have garnered as much interest as the reaction of dinitrogen pentoxide (N_2O_5) at aqueous

interfaces, as this reaction has been shown to be highly sensitive to surface chemical composition,[3–5] phase,[5,6] and the presence of surfactants.[7–13] In the atmosphere, accurate representation of the lifetime of N_2O_5 is of importance; N_2O_5 serves as both a nocturnal reservoir for nitrogen oxides ($NO_x \equiv NO + NO_2$) and a pathway for the production of photolabile halogen species such as nitryl chloride ($ClNO_2$).[14–16]

The efficiency of N_2O_5 reactive uptake at an aqueous interface is commonly reported as the reactive uptake coefficient, $\gamma(N_2O_5)$, or the reaction probability per N_2O_5 collision with an aerosol particle. The concerted reaction mechanism that controls $\gamma(N_2O_5)$, as described in the reaction sequence below, begins with mass accommodation of N_2O_5 to the particle surface. Following accommodation, autoionization of N_2O_5 results in the formation of a highly reactive nitronium ion (NO_2^+) intermediate (R2), which can react with water to form NO_3^- (R3), Cl^- to form $ClNO_2$ (R4), or a host of other nucleophiles (e.g, aromatic compounds).[17–20]

$$N_2O_5\,(g) \leftrightarrow N_2O_5\,(aq) \quad \text{(R1)}$$

$$N_2O_5\,(aq) \leftrightarrow NO_2^+\,(aq) + NO_3^-\,(aq) \quad \text{(R2)}$$

$$NO_2^+\,(aq) + H_2O\,(l) \leftrightarrow 2H^+\,(aq) + NO_3^-\,(aq) \quad \text{(R3)}$$

$$NO_2^+\,(aq) + Cl^-\,(aq) \leftrightarrow ClNO_2\,(aq) \quad \text{(R4)}$$

$$ClNO_2\,(aq) \leftrightarrow ClNO_2\,(g) \quad \text{(R5)}$$

Recent studies have focused on the role the organic fraction plays in altering $\gamma(N_2O_5)$, through either a reduction in the entry probability of N_2O_5 due to the presence of a surfactant film, [7,11] or a diffusive limitation in N_2O_5 transport from the interface to the aqueous core of the particle.[8,9,21] Ambient studies such as Bertram et al. 2009 report a strong anti-correlation between $\gamma(N_2O_5)$ and the particulate organic to sulfate ratio, consistent with the picture of a phase separated organic film.[21,22] Using aircraft observations, Brown et al. observed up to a factor of ten decrease in $\gamma(N_2O_5)$ correlated with an increase in particulate organic content during ambient measurements in the northeastern United States.[23] Laboratory studies using both smog chambers and molecular mimics have demonstrated that organic films exhibiting monolayer coverage can serve to reduce $\gamma(N_2O_5)$ by more than a factor of 60.[8] Escorcia et al. observed up to nearly a factor of 50 reduction in $\gamma(N_2O_5)$, dependent on the mass fraction of α-pinene oxidation products in mixed secondary organic aerosol containing ammonium bisulfate.[3] The authors attribute the suppression in $\gamma(N_2O_5)$ to either an organic-induced reduction in the mass accommodation coefficient, or decrease in the rate of N_2O_5 dissolution and diffusion in the particle bulk post-accommodation. Parallel studies have focused on the role of surfactant monolayers in suppressing $\gamma(N_2O_5)$, where straight chain

surfactants have been shown to suppress $\gamma(N_2O_5)$ by as much as a factor of 60 when compared to the sub-phase alone.[8] In contrast, no suppression in $\gamma(N_2O_5)$ was observed for branched organic surfactants such as phytanic acid, suggesting that the degree of organic packing on the reactive surface governs the ability of N_2O_5 to reach the reactive sub-phase. A 3.5 wt% solution, equal to a monolayer coverage of sodium dodecyl sulfate on aqueous NaCl particles, was found to suppress the reactive uptake of N_2O_5 by a factor of ten,[7] while a monolayer coverage of a shorter chain organic, hexanoic acid, on artificial seawater aerosol reduced $\gamma(N_2O_5)$ by as much as a factor of four.[11]

Here, we focus on the role that organics present in nascent sea spray aerosol (SSA) particles play in altering $\gamma(N_2O_5)$. It has been shown that sub-micrometer sized SSA particles can contain large organic mass fractions (0.17-0.83).[24–26] The observed range in organic mass fraction is inconsistent with the early conceptual representation of SSA as salty particulates with well-ordered surfactant films at the surface,[27,28] and more consistent with either a thick organic film or an internally mixed inorganic/organic particle.

The abundance and composition of the organic mass fraction of SSA is critically linked to the biological, chemical, and physical processes occurring in the surface ocean.[24–26] Specifically, the inter-related life cycle of phytoplankton, bacteria, and viruses, referred to as the microbial loop,[29–32] serves to enhance and transform organic material in surface waters. The primary stages of the microbial loop include an increase in phytoplankton abundance, followed by a subsequent increase in bacterial concentrations commensurate with phytoplankton decay. Bacteria number concentrations eventually decay due to virus grazing, resulting in a spike in virus count. As a result of species cycling, the concentration and speciation of biologically-derived organic material also varies based on the stage of the phytoplankton bloom. It has been suggested[26,33] that the composition and mass fraction of organics in SSA particles will track the biological and chemical evolution of a phytoplankton bloom. In this paper, we utilize molecular mimics for organic species, representative of those found in the ocean during a phytoplankton bloom, to assess the impact of SSA chemical composition on the reactive uptake of N_2O_5. These results are compared to N_2O_5 uptake values obtained from SSA generated from natural ambient seawater and particles sampled during clean marine conditions at the Scripps Institution of Oceanography (SIO) Pier.[20,34]

3. Materials and Methods

3.1 N_2O_5 generation and detection N_2O_5 was generated *in situ* as described previously.[35] Briefly, ozone, generated by flowing UHP zero air over an exposed UV mercury Penray lamp (Jelight, Irvine, CA), is mixed with NO_2. The combined flows are allowed to mix in a glass mixing cell for approximately two

minutes, after which the total flow is 100 sccm and is delivered *via* 1/8" PFA tubing to the entrained aerosol flow reactor. Guided by the initial work of Bertram et al. 2009, the mixing ratios at the flow reactor entrance were approximately: $[NO_2]$ = 290 ppb, $[O_3]$ = 30 ppb, $[N_2O_5]$ = 1 ppb. The reaction was run at room temperature (ca. 295K), resulting in a $[N_2O_5]$:$[NO_3]$ ratio greater than 50. The mixing ratio of HNO_3 at the flow reactor exit was estimated to be 10% that of N_2O_5, based on known ion-molecule reaction rates for I^- ion chemistry.[36]

The aerosol flow reactor closely resembles that described in Bertram et al., 2009.[35] The reactor is a 15 cm I.D., 90 cm long stainless steel tube. Prior to entering the flow reactor, aerosols are conditioned to a relative humidity between 39-65% by varying the exposure time of the aerosol-laden air within a desiccator and measuring the RH at the exit of the desiccator. Similar to Bertram et al. 2009, the particle stream was sent either directly to the flow tube or first through a filter assembly equipped with a Whatman supported PTFE membrane filter (Whatman, 5.0 μm, TE 38) to remove particles from the air stream. The valve assembly was controlled autonomously *via* computer controlled pneumatically actuated valves. The particle inlet to the reactor is located orthogonal to the flow tube and N_2O_5 reagent gas delivery to maximize mixing between the N_2O_5 gas and the particle-laden air flow in the entry region. The top of the reactor was equipped with a RH and temperature meter (Vaisala, HMP60 Humidity and Temperature Probe). The bottom cap of the flow tube was equipped with a similar port that allowed for exit of gases and reacted particles through a 1/4" Teflon tube to the inlet of the chemical ionization quadrupole mass spectrometer (CI-QMS). The flow rate of the reactor was 1800 sccm, which was set by a critical orifice in the front end of the CI-QMS, establishing an average reaction time of 615 s.

N_2O_5 and $ClNO_2$ concentrations were monitored continuously with a CI-QMS utilizing $I^-(H_2O)_n$ reagent ion chemistry.[37] N_2O_5 was measured directly as the $I^-(N_2O_5)$ adduct at 235 m/z, and $ClNO_2$ as the $I^-(ClNO_2)$ adduct at 208 and 210 m/z. Routine measurements of HNO_3 were also made by measuring the signal intensity at 189 m/z, which corresponds to $I^-(HNO_3)$. Data were collected at 1 Hz.

3.2 Sea spray aerosol generation and duty cycle Sea spray aerosol was generated using a Marine Aerosol Reference Tank (MART) described in detail in Stokes et al. 2013.[38] Briefly, a 210 L acrylic tank is filled with 120 L of either artificial seawater, or natural seawater obtained directly from the ocean. The MART is equipped with a recirculating water pump that generates an in tank plunging water sheet. The plunging water sheet, permitting the formation of subsurface bubble plumes and surface foam patches that accurately mimic those observed in the open ocean from breaking waves.[26,38] To allow for representative surface foam lifetime and dissipation rates, the plunging sheet was modulated in a 10s on, 6s off duty

cycle, referred to here as the "SSA production mode". During SSA production mode, the MART system produces aerosol continuously with consistent surface area distributions, as shown in Figure 1. Typical particle number, surface area, and mass concentrations from the MART can be found in Stokes et al., and correspond to total particle number and surface area concentrations of 6000-8000 cm^{-3} and 4500 - 6000 μm^2 cm^{-3}, depending on the flow rate through the MART.[38] Given the large headspace volume (90 L) and slow flow rates (3 slpm), the SSA production mode plunging modulation is not resolvable, and thus does not impact the resulting aerosol measurements.

For the experiments described here, the SSA production mode duty cycle was computer controlled, permitting autonomous operation. Following each organic addition, the headspace of the MART was purged with wet UHP nitrogen, created by flowing N_2 through a water bubbler. The system was run with the plunging sheet off for at minimum 60 minutes to ensure full purging of any ambient particles in the MART system. Following this, the SSA production mode was initialized and continued as described above for one hour. During this time, flow from the MART passed through the particle filter prior to reaching the flow reactor to allow the walls to equilibrate with the relative humidity. N_2O_5 was continuously generated and added to the flow reactor, regardless of the filter state. Fifteen minutes prior to the end of the SSA production mode, the filter is turned off, and the aerosol laden air flow is directed into the flow reactor to equilibrate the reactor walls with particles. At the conclusion of the SSA production mode, plunging is arrested in the MART (Fig. 2A), after which total particle number concentrations decay to zero as the headspace of the MART is depleted in SSA.[38] This part of the cycle is referred to as "SSA decay mode". SSA decay mode persists for 60 minutes, after which time the SSA production mode resumes, and the flow tube flow is returned to the filter state. This complete, 2 hour cycle was repeated three times for each water matrix studied. The complete cycle is shown in Figure 2 alongside corresponding changes in total particle surface area (red), and sub-micrometer particle surface area (green). As shown in Figure 2, the decay in particle concentration within the MART is size dependent, with larger particles exhibiting a shorter lifetime than smaller particles within the headspace.[38] The size dependent loss rate can be used to isolate sub-micrometer particles from super-micrometer particles for study of the loss of N_2O_5 to sub-micrometer aerosol as size dependent differences in particle chemical composition are expected.

3.3 Molecular mimics of seawater organics Two separate experiments were conducted in the MART as part of this study: 1) a synthetic microbial loop, designed to chemically replicate the microbial loop, was carried out in the MART, and 2) the MART was filled with ambient ocean water collected from Scripps Institution of Oceanography Pier. The first experiment involved filling the tank with an artificial seawater,

created by mixing MilliQ water and a sea salt mixture (Sea Salts, Sigma Aldrich, S9883) to create a matrix with ocean-relevant ion concentrations. Following the theoretical modeling studies of Burrows et al., we represent different stages of a phytoplankton bloom with five different classes of biologically-derived organic species.[39] Ocean concentrations of total organic carbon are on average 60-70 μM C.[40] However, concentrations are expected to be enhanced at the air-sea interface, producing much higher organic concentrations than in the average ocean state. The artificial seawater matrix was sequentially doped with 70 μM C of each of the following organic constituents: cholesterol (3β-Hydroxy-5-cholestene, Sigma Aldrich, C8667), galactose (D (+) galactose, Sigma Aldrich, G0750), lipopolysaccharides (lipopolysaccharides from Escherichia coli 0111:B4, Sigma Aldrich, L4130), albumin protein (Bovine Serum Albumin, Sigma Aldrich, A2153), and 1,2-dipalmitoyl-sn-glycero-3-phosphate monosodium salt (DPPA, Avanti Polar Lipids Inc., #830855P). N_2O_5 uptake coefficient measurements were made following the addition of each organic compound.

The organic mimics are listed in order of addition to the water matrix in Table 1, along with their molecular weight, carbon to oxygen ratio, and solubility. The first 70 μM organic addition was cholesterol, a species that has been previously detected in both the sea-surface microlayer (SSML) (enriched by up to 15 times) and SSA, and originates primarily from phytoplankton, as noted by Hardy, 1982 and references therein.[41] Following this, galactose was added to mimic sugars that have been detected during the growth of bacteria.[42] The third addition was lipopolysaccharides, which are found in the cell membranes of gram negative bacteria[43] and are often used as a measure of bacterial concentrations in ocean waters. [E.g.44,45] To represent protein and lipids also found in seawater, albumin protein and DPPA were added in 70 μM concentrations to the water matrix sequentially.

In the second experiment, the MART system was purged and filled with Pacific Ocean water obtained from the end of Scripps Institution of Oceanography Pier (La Jolla, CA, September 9th 2013). The water was not doped with any additional constituents, and was run as obtained from the ocean without filtering.

3.4 Seawater and sea spray aerosol characterization

3.4.1 Aerosol particle characterization Dry aerosol particle number and surface area distributions were measured in real time, during all experiments, using an Aerosol Particle Sizer (APS, TSI model 3321), measuring particles from 0.4 to 14 μm, and an Ultra High Sensitivity Aerosol Spectrometer (UHSAS, Droplet Measurement Technologies) sizing particles between 0.06 and 1 μm. Particle growth factors were determined *via* an optical closure procedure as previously described[26,46,47] and applied to the sizing data

for use in the calculation of $\gamma(N_2O_5)$ as the particle stream flowing to the sizing instruments was dried to < 10% RH.

Following the third and final SSA decay mode for each water matrix, size segregated SSA were generated and collected onto silicon nitride (Si_3N_4) window substrates housed in a micro-orifice uniform-deposit impactor (MOUDI). Particles were not dried prior to collection, and based on the rates of the sample and dilution flow, the RH at impaction is estimated to be ca. 60%. Two MOUDI stages (stage 5 and 7) were analyzed in detail. Particles collected on stage 5 correspond to wet particle diameters between 1-1.8 μm and particles collected on stage 7 correspond to wet particle diameters between 0.33-0.56 μm. Work presented here focuses on the stage 7 substrates as they most closely map the surface area maximum for sub-micrometer aerosol analyzed in the flow reactor.

The stage 7 substrates were imaged using Atomic Force Microscopy (AFM) to estimate the organic volume fraction of approximately 50 particles for each water matrix sample. AFM imaging was performed with a Molecular Force Probe 3D AFM (Asylum Research, Santa Barbara, CA). Alternating current (AC) mode images were collected at room RH (20-21%) with silicon probes (MikroMasch, Model CSC37) with a nominal spring constant of 0.35 N/m and a typical tip radius of curvature of 8-10 nm. Height, amplitude, and phase images were used to create particle masks over both the core and whole particle and a particle analyzer was used to determine the volume of the masked areas. Organic volume fraction was calculated as the volume of the whole particle minus the core volume, divided by the total particle volume, as described further in Section 4. Particle diameters post-impaction were measured using AFM analysis and the average measured diameters under 20% RH are reported here.

The total volume of the particle (V_{tot}) and the volume of the particle core (V_{core}) were directly quantified via AFM imaging. The organic coating volume (V_{coat}) is calculated by taking the difference of the total particle and core volume ($V_{coat} = V_{tot} - V_{core}$), assuming total phase separation. Additionally, the volume equivalent diameter of the particle core can be determined from the volume of the particle core ($d_{core} = 2 \times ((0.75\pi \times V_{core})^{1/3})$. Finally, calculated volume equivalent d_{core} and d_{AFM} can be used to estimate the thickness of the organic coating on the particle ($th_{coat} = (d_{AFM} - d_{core})/2$). This calculation was performed for each particle type, and the average diameter determined by AFM and calculated film thicknesses are shown in Table 2. Within the assumptions made for this calculation, including extrapolation of the measured AFM diameter to a spherical particle, ignoring any spreading of the particle that may have resulted from impaction onto the surface, and the assumption of phase separation of the organics and core,

the film thickness determined is remarkably consistent across all samples and is around 8 nm (at 20% RH).

Additionally, the organic mass fraction of the particles was estimated from the organic volume fraction determination. For this calculation, it was assumed the particle core had the same density as NaCl (2.2×10^{-12} g μm^{-3}), and due to the unknown phase of the organic fraction, a density between that of graphite and oil (1.6×10^{-12} g μm^{-3}) was used.[48,49]

3.4.2 Water Characterization Water samples were taken by skimming the top of the water surface with a clean media bottle following each organic addition. Surface tension was measured by agitating the water sample bottles and then transferring collected water into a clean glass dish provided with the Kruss Tensiometer K11 instrument. Here the Wilhelmy plate method was utilized for the surface tension measurements. Water pH was measured from the collected water samples using a pH meter (IQ Scientific Instruments pH/mV/thermometer #1506471).

3.5 Determination of $\gamma(N_2O_5)$ Traditional measurements of heterogeneous reaction rates using entrained aerosol flow reactors have focused on measuring the decay in reactant concentration at a fixed surface area concentration by varying the interaction time of the gas with the particles. The reactive uptake coefficient is often then calculated from the slope of the linear regression analysis for the dependence of the heterogeneous loss rate on particle surface area (S_a).[2,5,8,50,51] Here, we utilize a fixed gas-particle interaction time and calculate k_{obs} as a function of the N_2O_5 concentration in the presence and absence of aerosol particles (E1) as was done in Bertram et al., 2009, effectively yielding an instantaneous measure of k_{obs}. As discussed above, we induce a slow decay in particle surface area entering the flow reactor by arresting particle production in the MART.

The MART experiment was designed to include the particle decay mode for two purposes: 1) the decay in S_a provides a method for calculating the dependence of the heterogeneous loss rate on S_a, autonomously, and 2) the removal rate of SSA within the MART is strongly size dependent, as shown in Stokes et al. 2013, where super-micrometer particles are removed more quickly than sub-micrometer particles. This permits us to time gate our analysis to focus on sub-micrometer aerosol. Figure 4 shows a typical duty cycle during this experiment, including the corresponding change in the N_2O_5 signal (Fig. 4A). Total surface area is constant to within 12% during SSA production mode (Fig 4B). As shown in Figure 4B, when plunging is arrested (time = 0 s), super-micrometer particle surface area decays promptly, and by 500s the super-micrometer contribution to the total surface area concentration is less than 1%. For the

analysis described below, we constrain our sampling window to the period where the time rate of change in surface area is slower than the residence time of the flow reactor. In this analysis we only consider periods where the surface area does not vary by more than 20% over the residence time of the flow reactor.

During the SSA decay mode, the N_2O_5 signal increases due to the decreasing surface area available for reaction as RH is held constant during the decay. Due to the delay in signal response resulting from the residence time in the flow tube, the particle surface area data and N_2O_5 signal were temporally adjusted to match the beginning of the particle decay mode. We first average the N_2O_5 signal intensities to 20 seconds to match the averaging time of the particles surface area measurements. Each N_2O_5 average point during the particle decay period was then divided by the maximum N_2O_5 signal in the decay period (corresponding to the point of S_a = 0 μm^2 cm^{-3}). Lastly, the instantaneous observed loss rate (k_{obs}) was calculated using Equation 1 for each 20 s averaging period as:

$$k_{obs} = -\frac{1}{\tau} \times \ln\left(\frac{(N_2O_5)_{time=t}}{(N_2O_5)_{max}}\right) \quad \text{E1}$$

where τ is the residence time in the flow reactor (615 s), $(N_2O_5)_t$ are the individual N_2O_5 time averaged points during particle decay in the reactor, and $(N_2O_5)_{max}$ is the highest N_2O_5 value during the period. A key point here is that S_a is not changing during each determination of k_{obs}.

The reactive uptake coefficient, γ(N_2O_5), was calculated as the slope of a plot of instantaneous k_{obs} (Equation 2) as a function of total surface area (S_a).

$$k_{obs} = \left(\left(\frac{\gamma \times \omega}{4}\right) \times S_a\right) + k_{wall} \quad \text{E2}$$

where ω is the mean speed of N_2O_5 (241.7 m/s), and k_{wall} is the loss rate of N_2O_5 to the flow reactor wall. This method of γ(N_2O_5) determination is illustrated in Figure 5, where the black line is a one-sided linear fit to the data providing the slope, which is indicated as γ(N_2O_5) in the legend. The y-axis intercept is k_{wall}. Additionally, grey lines indicating specific gamma values are shown for reference. At present, it is not clear what is causing the steeping in the slope, corresponding to a particle surface area of 150 μm^{2}cm^{-3}, however at this low surface area the differences between N_2O_5 concentrations between the particle on and

301 off states in E1 are less than 5%, and minor fluctuations in k_{wall} and the N_2O_5 source have a large impact
302 on the retrieved k_{obs}.
303
304 **4. Results and Discussion**
305 **4.1 Aerosol organic volume fraction** SSA particles were analyzed with AFM to determine the organic
306 volume fraction for particle populations collected from each water matrix. Distributions of organic
307 volume fraction measured per water matrix are shown in Figure 6. The halo of material surrounding the
308 cubic particle core is assigned as organic content here, however, this fraction may also contain inorganic
309 constituents such as Mg^{2+}, Ca^{2+}, and K^{+}.[52] As such, the organic volume fractions reported here represent
310 an upper limit.
311
312 Organic volume fractions were determined for each stage of the experiment. For the salt water tank, the
313 average organic volume fraction was 0.05 ± 0.05, not purely 0, due to the fact that Sigma Aldrich sea salts
314 are obtained via natural sea water evaporation, rather than from ACS reagent grade salt mixture, and thus
315 contain some degree of organic components. Following the addition of cholesterol (70 μM C), the mean
316 organic volume fraction was 0.10 ± 0.05. Upon the addition of 70 μM C galactose, the mean organic
317 volume fraction increased to 0.18 ± 0.06. For all subsequent organic additions, the mean particle organic
318 volume fraction stayed in a narrow range of 0.19-0.21.
319
320 Figure 6F indicates that particles generated from natural seawater show a narrower organic volume
321 fraction distribution, with a standard deviation of 0.03, yet with a very similar average value (0.18) to
322 samples post-galactose addition, which ranged from 0.18-0.21. These values are listed in Table 2. Within
323 error, the organic volume fraction values for the synthetic bloom water matrix (post-cholesterol addition)
324 and the real ocean sample are consistent with values stated previously in the literature for hydrophobic
325 organic volume fractions for similar sized aerosol derived from real ocean water samples (0.20-0.29
326 organic volume fraction for particles up to 246 nm, wet diameter).[53]
327
328 **4.2 Effect of marine organic mimics on $\gamma(N_2O_5)$** For both the synthetic bloom and ambient seawater
329 systems, a minimum of three to a maximum of eight determinations of $\gamma(N_2O_5)$ were made for each water
330 matrix. These values were averaged and the resulting $\gamma(N_2O_5)$ is reported in Table 2, along with the range
331 of values measured during each water matrix, the relative humidity range measured in the flow reactor,
332 and the measured pH and surface tension of water samples collected from each water matrix. The
333 propagated error with any individual $\gamma(N_2O_5)$ value (not shown) is significantly less than the range in

$\gamma(N_2O_5)$ observed. The uncertainty in any individual determination of $\gamma(N_2O_5)$ is primarily limited by variability in the N_2O_5 source concentration as was the case in Bertram et al., 2009.

To assess the dependence of $\gamma(N_2O_5)$ on the composition of the water matrix from which SSA was generated, $\gamma(N_2O_5)$ is shown as a function of the concentration of carbon in the water (Fig. 7A). The error bars indicate the range in $\gamma(N_2O_5)$ for a given condition. As shown in Fig. 7A, there is a slight increase in the mean $\gamma(N_2O_5)$ following the addition of LPS ([C] = 210 μM). However, the variability in $\gamma(N_2O_5)$, as indicated by the error bars in Fig. 7A, overlaps with the adjacent $\gamma(N_2O_5)$ determinations. It should also be noted that the 70 μM addition of cholesterol results in an average $\gamma(N_2O_5)$ similar to that of the real ocean water sample.

Beyond variability in carbon concentrations, water samples collected from the MART exhibited a wide range in surface tension (52.6 - 69 mN m^{-1}), consistent with the addition of the organic molecules. The surface tension, as measured following the addition of Sigma Aldrich sea salts at ocean concentrations was 68.7 mN m^{-1}, significantly less that that expected for a 0.5 M NaCl solution (73 mN m^{-1}).[54] This is a result of trace organic compounds present in the sea salts mixture that is produced from the evaporation of natural seawater. The addition of albumin to the MART resulted in both the largest suppression in surface tension (52.6 mN m^{-1}) as well as the generation of significant standing foam. Prior to the addition of DPPA, the standing foam dissipated, suggesting that albumin had been scavenged from the MART either by direct uptake to the interior surfaces of the MART (walls and recirculating pump) and/or release to the atmosphere as particulates. While not measured, it is expected that the surface tension would have increased during this period. The albumin trial lasted an extended period of time (6 days as compared to 1 day for the other additions) due to an instrumental issue. Despite the large percent changes in surface tension, no statistically relevant change in $\gamma(N_2O_5)$ was detected. Bulk water pH was measured throughout the experiments and $\gamma(N_2O_5)$ is shown as a function of water pH in Fig. 7C. The water side pH for the synthetic experiment ranged from 7.74 for sea salts in MilliQ water to 8.15 after the addition of all organics. The pH of the collected ocean water was 7.87, similar to the pH values after the addition of cholesterol, galactose, and LPS (see Table 2). Despite the range of pH values, $\gamma(N_2O_5)$ was found to be invariable with water pH.

As shown in Figure 8, there was also no clear dependence of $\gamma(N_2O_5)$ on particle organic volume fraction or film thickness. This suggests that under the sampling conditions of this study (RH > 50%), organic material was likely well mixed within the particle, thus permitting prompt diffusion of N_2O_5 throughout

the particle. Further, we see no evidence for a surfactant monolayer that serves to block N_2O_5 entry into the particle. It is important to note that the calculation of the volume fraction and film thickness were done at 20% RH, while determinations of $\gamma(N_2O_5)$ were conducted between 50-65% RH. As a result the presence of an organic film may or may not be present under the conditions that the reactive uptake coefficient were measured. Future work in this area will focus on determining $\gamma(N_2O_5)$ and film thickness as a function of RH, as we may expect to see deviations from the relationships shown in Figure 8 at lower RH.

4.3 Determinations of $\gamma(N_2O_5)$ for nascent SSA Determinations of $\gamma(N_2O_5)$ for SSA particles generated in the MART from coastal seawater also show no indication that organics present in nascent SSA significantly suppress N_2O_5 reactivity ($\gamma(N_2O_5)$ = 0.0065 - 0.0147), relative to that for sea salts ($\gamma(N_2O_5)_{sea\ salts}$ =0.0077 - 0.0372), at relative humidity above 50% (Fig. 8). This suggests that organics present in SSA particles do not impede N_2O_5 entry or diffusion following accommodation under the conditions sampled here. These results are consistent with those observed by Cosman et al., who showed that coating particles with branched chain organics showed no significant impact on $\gamma(N_2O_5)$, likely related to the surface packing density of branched organics on the particle surface.[8] Similarly, the organic molecules used in the synthetic bloom experiments in this study (e.g., LPS) are unlikely to pack tightly on the surface of particles due to their complex structures. Given the large organic volume fractions measured for MART generated particles (> 0.15), it is plausible that a larger effect of organics on $\gamma(N_2O_5)$ may exist at lower relative humidity, as has been suggested by laboratory studies of secondary organic aerosol.[6,11]

The collection of measurements described in this paper are shown in Figure 9 alongside previous ambient determinations of $\gamma(N_2O_5)$ made from the SIO pier.[20,34] Determinations of $\gamma(N_2O_5)$ observed in this study agree with those measured for ambient particles with similar organic mass fractions. As illustrated in Figure 9, significant suppression in $\gamma(N_2O_5)$ for ambient particulates is not achieved until much higher organics mass fractions. As was discussed in Riedel et al., the air masses associated with these particles were of continental origin and contained high nitrate content, which served to reduce $\gamma(N_2O_5)$.[34]

5. Conclusions

The results presented here indicate that organic material present in nascent sea spray aerosol sampled here does not serve to impede the reactive uptake of N_2O_5 at RH greater than 50%. Further, we observe no evidence for the suppression in the reactive uptake of N_2O_5 to SSA generated from a host of marine organic mimics at ocean relevant concentrations for RH greater than 50%. For waterside carbon

concentrations ranging between 70-350 μM, the organic volume fraction as measured using AFM remained between 0.10-0.21 and $\gamma(N_2O_5)$ remained between 0.013-0.031. The results presented here suggest that either: 1) surface active material at the air-particle interface does not pack as tightly as monolayers of single component straight chain carboxylic acids, thus allowing for N_2O_5 access to the aqueous core for reaction and/or 2) organic material in nascent SSA is either well mixed within the particle under the RH conditions sampled here, thus permitting prompt diffusion of N_2O_5 throughout the particle, or organic material is present at the interface but at insufficient amount to impact the reactivity. Future work in this area will focus on coincident determinations of organic film thickness and N_2O_5 reaction probability as a function of relative humidity.

6. Acknowledgements

This research was supported by the National Science Foundation *via* the Center for Aerosol Impact on Climate and the Environment, a Center for Chemical Innovation (NSF CHE1305427). The authors also thank Steven Schill for participation and helpful discussions during the MART experiments. O.S.R gratefully acknowledges a Graduate Research Fellowship from the National Science Foundation (2011-2014).

7. References

(1) Morris, E. D.; Niki, H. Reaction of Dinitrogen Pentoxide with Water. *J. Phys. Chem.* **1973**, *77* (16), 1929–1932.

(2) Mozurkewich, M.; Calvert, J. G. Reaction Probability of N2O5 on Aqueous Aerosols. *J. Geophys. Res. Atmospheres* **1988**, *93* (D12), 15889–15896.

(3) Escorcia, E. N.; Sjostedt, S. J.; Abbatt, J. P. D. Kinetics of N2O5 Hydrolysis on Secondary Organic Aerosol and Mixed Ammonium Bisulfate−Secondary Organic Aerosol Particles. *J. Phys. Chem. A* **2010**, *114* (50), 13113–13121.

(4) Gross, S.; Iannone, R.; Xiao, S.; Bertram, A. K. Reactive Uptake Studies of NO3 and N2O5 on Alkenoic Acid, Alkanoate, and Polyalcohol Substrates to Probe Nighttime Aerosol Chemistry. *Phys. Chem. Chem. Phys. PCCP* **2009**, *11* (36), 7792–7803.

(5) Griffiths, P. T.; Badger, C. L.; Cox, R. A.; Folkers, M.; Henk, H. H.; Mentel, T. F. Reactive Uptake of N2O5 by Aerosols Containing Dicarboxylic Acids. Effect of Particle Phase, Composition, and Nitrate Content. *J. Phys. Chem. A* **2009**, *113* (17), 5082–5090.

(6) Thornton, J. A.; Braban, C. F.; Abbatt, J. P. D. N2O5 Hydrolysis on Sub-Micron Organic Aerosols: The Effect of Relative Humidity, Particle Phase, and Particle Size. *Phys. Chem. Chem. Phys.* **2003**, *5* (20), 4593–4603.

(7) McNeill, V. F.; Patterson, J.; Wolfe, G. M.; Thornton, J. A. The Effect of Varying Levels of Surfactant on the Reactive Uptake of N2O5 to Aqueous Aerosol. *Atmos Chem Phys* **2006**, *6* (6), 1635–1644.

(8) Cosman, L. M.; Knopf, D. A.; Bertram, A. K. N2O5 Reactive Uptake on Aqueous Sulfuric Acid Solutions Coated with Branched and Straight-Chain Insoluble Organic Surfactants. *J. Phys. Chem. A* **2008**, *112* (11), 2386–2396.
(9) Anttila, T.; Kiendler-Scharr, A.; Tillmann, R.; Mentel, T. F. On the Reactive Uptake of Gaseous Compounds by Organic-Coated Aqueous Aerosols: Theoretical Analysis and Application to the Heterogeneous Hydrolysis of N2O5. *J. Phys. Chem. A* **2006**, *110* (35), 10435–10443.
(10) Folkers, M.; Mentel, T. F.; Wahner, A. Influence of an Organic Coating on the Reactivity of Aqueous Aerosols Probed by the Heterogeneous Hydrolysis of N2O5. *Geophys. Res. Lett.* **2003**, *30* (12), 1644.
(11) Thornton, J. A.; Abbatt, J. P. D. N2O5 Reaction on Submicron Sea Salt Aerosol: Kinetics, Products, and the Effect of Surface Active Organics. *J. Phys. Chem. A* **2005**, *109* (44), 10004–10012.
(12) Knopf, D. A.; Cosman, L. M.; Mousavi, P.; Mokamati, S.; Bertram, A. K. A Novel Flow Reactor for Studying Reactions on Liquid Surfaces Coated by Organic Monolayers: Methods, Validation, and Initial Results. *J. Phys. Chem. A* **2007**, *111* (43), 11021–11032.
(13) Park, S.-C.; Burden, D. K.; Nathanson, G. M. The Inhibition of N2O5 Hydrolysis in Sulfuric Acid by 1-Butanol and 1-Hexanol Surfactant Coatings. *J. Phys. Chem. A* **2007**, *111* (15), 2921–2929.
(14) Finlayson-Pitts, B. J.; Ezell, M. J.; Pitts, J. N. Formation of Chemically Active Chlorine Compounds by Reactions of Atmospheric NaCl Particles with Gaseous N2O5 and ClONO2. *Nature* **1989**, *337* (6204), 241–244.
(15) Osthoff, H. D.; Roberts, J. M.; Ravishankara, A. R.; Williams, E. J.; Lerner, B. M.; Sommariva, R.; Bates, T. S.; Coffman, D.; Quinn, P. K.; Dibb, J. E.; et al. High Levels of Nitryl Chloride in the Polluted Subtropical Marine Boundary Layer. *Nat. Geosci.* **2008**, *1* (5), 324–328.
(16) Roberts, J. M.; Osthoff, H. D.; Brown, S. S.; Ravishankara, A. R.; Coffman, D.; Quinn, P.; Bates, T. Laboratory Studies of Products of N2O5 Uptake on Cl− Containing Substrates. *Geophys. Res. Lett.* **2009**, *36* (20), L20808.
(17) Wahner, A.; Mentel, T. F.; Sohn, M.; Stier, J. Heterogeneous Reaction of N2O5 on Sodium Nitrate Aerosol. *J. Geophys. Res. Atmospheres* **1998**, *103* (D23), 31103–31112.
(18) Mentel, T. F.; Sohn, M.; Wahner, A. Nitrate Effect in the Heterogeneous Hydrolysis of Dinitrogen Pentoxide on Aqueous Aerosols. *Phys. Chem. Chem. Phys.* **1999**, *1* (24), 5451–5457.
(19) Heal, M. R.; Harrison, M. A. J.; Neil Cape, J. Aqueous-Phase Nitration of Phenol by N2O5 and ClNO2. *Atmos. Environ.* **2007**, *41* (17), 3515–3520.
(20) Ryder, O. S.; Ault, A. P.; Cahill, J. F.; Guasco, T. L.; Riedel, T. P.; Cuadra-Rodriguez, L. A.; Gaston, C. J.; Fitzgerald, E.; Lee, C.; Prather, K. A.; et al. On the Role of Particle Inorganic Mixing State in the Reactive Uptake of N2O5 to Ambient Aerosol Particles. *Environ. Sci. Technol.* **2014**, *48* (3), 1618–1627.
(21) Gaston, C. J.; Thornton, J. A.; Ng, N. L. Reactive Uptake of N2O5 to Internally Mixed Inorganic and Organic Particles: The Role of Organic Carbon Oxidation State and Inferred Organic Phase Separations. *Atmos Chem Phys* **2014**, *14* (11), 5693–5707.
(22) Bertram, T. H.; Thornton, J. A.; Riedel, T. P.; Middlebrook, A. M.; Bahreini, R.; Bates, T. S.; Quinn, P. K.; Coffman, D. J. Direct Observations of N2O5 Reactivity on Ambient Aerosol Particles. *Geophys. Res. Lett.* **2009**, *36* (19), L19803.
(23) Brown, S. S.; Ryerson, T. B.; Wollny, A. G.; Brock, C. A.; Peltier, R.; Sullivan, A. P.; Weber, R. J.; Dubé, W. P.; Trainer, M.; Meagher, J. F.; et al. Variability in Nocturnal Nitrogen Oxide Processing and Its Role in Regional Air Quality. *Science* **2006**, *311* (5757), 67–70.
(24) Facchini, M. C.; Rinaldi, M.; Decesari, S.; Carbone, C.; Finessi, E.; Mircea, M.; Fuzzi, S.; Ceburnis, D.; Flanagan, R.; Nilsson, E. D.; et al. Primary Submicron Marine Aerosol Dominated by Insoluble Organic Colloids and Aggregates. *Geophys. Res. Lett.* **2008**, *35* (17), L17814.

(25) O'Dowd, C. D.; Facchini, M. C.; Cavalli, F.; Ceburnis, D.; Mircea, M.; Decesari, S.; Fuzzi, S.; Yoon, Y. J.; Putaud, J.-P. Biogenically Driven Organic Contribution to Marine Aerosol. *Nature* **2004**, *431* (7009), 676–680.

(26) Prather, K. A.; Bertram, T. H.; Grassian, V. H.; Deane, G. B.; Stokes, M. D.; DeMott, P. J.; Aluwihare, L. I.; Palenik, B. P.; Azam, F.; Seinfeld, J. H.; et al. Bringing the Ocean into the Laboratory to Probe the Chemical Complexity of Sea Spray Aerosol. *Proc. Natl. Acad. Sci.* **2013**, *110* (19), 7550–7555.

(27) Gill, P. S.; Graedel, T. E.; Weschler, C. J. Organic Films on Atmospheric Aerosol Particles, Fog Droplets, Cloud Droplets, Raindrops, and Snowflakes. *Rev. Geophys.* **1983**, *21* (4), 903–920.

(28) Ellison, G. B.; Tuck, A. F.; Vaida, V. Atmospheric Processing of Organic Aerosols. *J. Geophys. Res. Atmospheres* **1999**, *104* (D9), 11633–11641.

(29) Russell, L. M.; Hawkins, L. N.; Frossard, A. A.; Quinn, P. K.; Bates, T. S. Carbohydrate-like Composition of Submicron Atmospheric Particles and Their Production from Ocean Bubble Bursting. *Proc. Natl. Acad. Sci.* **2010**, *107* (15), 6652–6657.

(30) Quinn, P. K.; Bates, T. S.; Schulz, K. S.; Coffman, D. J.; Frossard, A. A.; Russell, L. M.; Keene, W. C.; Kieber, D. J. Contribution of Sea Surface Carbon Pool to Organic Matter Enrichment in Sea Spray Aerosol. *Nat. Geosci.* **2014**, *7* (3), 228–232.

(31) Pomeroy, L.; leB. Williams, P.; Azam, F.; Hobbie, J. The Microbial Loop. *Oceanography* **2007**, *20* (2), 28–33.

(32) Azam, F. Microbial Control of Oceanic Carbon Flux: The Plot Thickens. *Science* **1998**, *280* (5364), 694–696.

(33) Wang, X.; Sultana, C. M.; Trueblood, J.; Hill, T. C. J.; Malfatti, F.; Lee, C.; Laskina, O.; Moore, K. A.; Beall, C. M.; McCluskey, C. S.; et al. Microbial Control of Sea Spray Aerosol Composition: A Tale of Two Blooms. *ACS Cent. Sci.* **2015**, *1* (3), 124–131.

(34) Riedel, T. P.; Bertram, T. H.; Ryder, O. S.; Liu, S.; Day, D. A.; Russell, L. M.; Gaston, C. J.; Prather, K. A.; Thornton, J. A. Direct N2O5 Reactivity Measurements at a Polluted Coastal Site. *Atmos Chem Phys* **2012**, *12* (6), 2959–2968.

(35) Bertram, T. H.; Thornton, J. A.; Riedel, T. P. An Experimental Technique for the Direct Measurement of N2O5 Reactivity on Ambient Particles. *Atmos Meas Tech* **2009**, *2* (1), 231–242.

(36) Huey, L. G. Measurement of Trace Atmospheric Species by Chemical Ionization Mass Spectrometry: Speciation of Reactive Nitrogen and Future Directions. *Mass Spectrom. Rev.* **2007**, *26* (2), 166–184.

(37) Kercher, J. P.; Riedel, T. P.; Thornton, J. A. Chlorine Activation by N2O5: Simultaneous, in Situ Detection of ClNO2 and N2O5 by Chemical Ionization Mass Spectrometry. *Atmos Meas Tech* **2009**, *2* (1), 193–204.

(38) Stokes, M. D.; Deane, G. B.; Prather, K.; Bertram, T. H.; Ruppel, M. J.; Ryder, O. S.; Brady, J. M.; Zhao, D. A Marine Aerosol Reference Tank System as a Breaking Wave Analogue for the Production of Foam and Sea-Spray Aerosols. *Atmos Meas Tech* **2013**, *6* (4), 1085–1094.

(39) Burrows, S. M.; Ogunro, O.; Frossard, A. A.; Russell, L. M.; Rasch, P. J.; Elliott, S. M. A Physically Based Framework for Modeling the Organic Fractionation of Sea Spray Aerosol from Bubble Film Langmuir Equilibria. *Atmos Chem Phys* **2014**, *14* (24), 13601–13629.

(40) Hansell, D.; Carlson, C.; Repeta, D.; Schlitzer, R. Dissolved Organic Matter in the Ocean: A Controversy Stimulates New Insights. *Oceanography* **2009**, *22* (4), 202–211.

(41) Hardy, J. T. The Sea Surface Microlayer: Biology, Chemistry and Anthropogenic Enrichment. *Prog. Oceanogr.* **1982**, *11* (4), 307–328.

(42) Benner, R.; Herndl, G. Bacterially Derived Dissolved Organic Matter in the Microbial Carbon Pump. In *Microbial Carbon Pump in the Ocean, N. Jiao, F. Azam, S. Sanders Eds.*; Science/AAAS: Washington, DC, 2011; p 46.

(43) Seltmann, G.; Holst, O. *The Bacterial Cell Wall*; Springer Science & Business Media, 2002.
(44) Nagata, T.; Fukuda, R.; Koike, I.; Kogure, K.; Kirchman, D. L. DEGRADATION BY BACTERIA OF MEMBRANE AND SOLUBLE PROTEIN IN SEAWATER. *Aquat. Microb. Ecol.* **1998**, *14* (1), 29–37.
(45) Maeda, M.; Lee, W. J.; Taga, N. Distribution of Lipopolysaccharide, an Indicator of Bacterial Biomass, in Subtropical Areas of the Sea. *Mar. Biol.* **1983**, *76* (3), 257–262.
(46) Zhang, X.; Massoli, P.; Quinn, P. K.; Bates, T. S.; Cappa, C. D. Hygroscopic Growth of Submicron and Supermicron Aerosols in the Marine Boundary Layer. *J. Geophys. Res. Atmospheres* **2014**, *119* (13), 2013JD021213.
(47) Atkinson, D. B.; Radney, J. G.; Lum, J.; Kolesar, K. R.; Cziczo, D. J.; Pekour, M. S.; Zhang, Q.; Setyan, A.; Zelenyuk, A.; Cappa, C. D. Aerosol Optical Hygroscopicity Measurements during the 2010 CARES Campaign. *Atmos Chem Phys* **2015**, *15* (8), 4045–4061.
(48) Royal Society of Chemistry. The Merck Index Online https://www.rsc.org/merck-index (accessed Nov 15, 2014).
(49) Haynes, W. M. *CRC Handbook of Chemistry and Physics, 95th Edition*; CRC Press, 2014.
(50) Stewart, D. J.; Griffiths, P. T.; Cox, R. A. Reactive Uptake Coefficients for Heterogeneous Reaction of N2O5 with Submicron Aerosols of NaCl and Natural Sea Salt. *Atmos Chem Phys* **2004**, *4* (5), 1381–1388.
(51) Fried, A.; Henry, B. E.; Calvert, J. G.; Mozurkewich, M. The Reaction Probability of N2O5 with Sulfuric Acid Aerosols at Stratospheric Temperatures and Compositions. *J. Geophys. Res. Atmospheres* **1994**, *99* (D2), 3517–3532.
(52) Ault, A. P.; Guasco, T. L.; Ryder, O. S.; Baltrusaitis, J.; Cuadra-Rodriguez, L. A.; Collins, D. B.; Ruppel, M. J.; Bertram, T. H.; Prather, K. A.; Grassian, V. H. Inside versus Outside: Ion Redistribution in Nitric Acid Reacted Sea Spray Aerosol Particles as Determined by Single Particle Analysis. *J. Am. Chem. Soc.* **2013**, *135* (39), 14528–14531.
(53) Park, J. Y.; Lim, S.; Park, K. Mixing State of Submicrometer Sea Spray Particles Enriched by Insoluble Species in Bubble-Bursting Experiments. *J. Atmospheric Ocean. Technol.* **2013**, *31* (1), 93–104.
(54) Jones, G.; Ray, W. A. The Surface Tension of Solutions of Electrolytes as a Function of the Concentration. III. Sodium Chloride. *J. Am. Chem. Soc.* **1941**, *63* (12), 3262–3263.
(55) Paumgartner, G. *Bile Acid Biology and Its Therapeutic Implications: Proceedings of the Falk Symposium 141 (XVIII Internationale Bile Acid Meeting) Held in Stockholm, Sweden, June 18 - 19, 2004*; Springer Science & Business Media, 2005.
(56) Gould, S. P. The Final Solubility of D-Galactose in Water. *J. Dairy Sci.* **1940**, *23* (3), 227.
(57) LPS-EB Standard lipopolysaccharide from E. coli 0111:B4 strain- TLR4 ligand http://www.invivogen.com/PDF/LPS_EB_TDS.pdf.
(58) ALBUMIN, BOVINE https://www.sigmaaldrich.com/content/dam/sigma-aldrich/docs/Sigma/Product_Information_Sheet/a4919pis.pdf.
(59) 16:0 PC (DPPC) 1,2-dipalmitoyl-sn-glycero-3-phosphocholine 850355 https://www.avantilipids.com/index.php?option=com_content&view=article&id=216&Itemid=206&catnumber=850355.

574 **Table 1:** Synthetic seawater components and their respective properties.

	Molecular Weight (g mol^{-1})	C:O	H:C	Water Solubility (mg mL^{-1})
Cholesterol	386.66	27:1	46:27	0.002 [55]
Galactose	180.16	1:1	2:1	684 [56]
Lipopolysaccharides	>3880.02	N/A	N/A	5[57]
Albumin	66kDa	N/A	N/A	40[58]
DPPA	670.87	4.4:1	1.9:1	insoluble[59]

575

Table 2: Average values of $\gamma(N_2O_5)$ obtained during each stage of the synthetic bloom, alongside the range of relative humidity, pH, and surface tension of the water matrix. The average particle organic volume fraction is determined *via* AFM measurements, and the organic film thickness is derived from the organic volume fraction estimates.

*AFM-derived at 20% RH

Stage	$\gamma(N_2O_5)$	$\gamma(N_2O_5)$ range	RH range (%)	Water pH	Surface tension (mN/m)	Avg. vol. equivalent particle diameter (nm) *	Avg. organic volume fraction	Calculated avg. organic coating thickness (nm)
0 (Salt)	0.0165	0.0077 - 0.0372	39 - 73	7.74	68.7	150 ± 110	0.05 ± 0.05	2.0 ± 0.4
1 (+ Sterol)	0.0129	0.0079 - 0.0215	54 - 60	7.90	68.7	210 ± 110	0.10 ± 0.06	4.1 ± 0.5
2 (+ Galactose)	0.0177	0.0134 - 0.0228	49 - 53	7.85	68.1	210 ± 110	0.18 ± 0.09	7.7 ± 0.4
3 (+ LPS)	0.0314	0.0108 - 0.0573	51 - 61	7.89	69.0	220 ± 70	0.21 ± 0.08	7.9 ± 0.4
4 (+ Albumin)	0.0140	0.0085 - 0.0179	56 - 65	8.16	52.6	230 ± 80	0.20 ± 0.05	8.5 ± 0.3
5 (+ DPPA)	0.0138	0.0097 - 0.0213	53 - 59	8.15	58.7	210 ± 100	0.19 ± 0.05	9.0 ± 0.2
Seawater	0.0116	0.0065 - 0.0147	53 - 59	7.87	63.5	210 ± 110	0.18 ± 0.04	8.1 ± 0.3

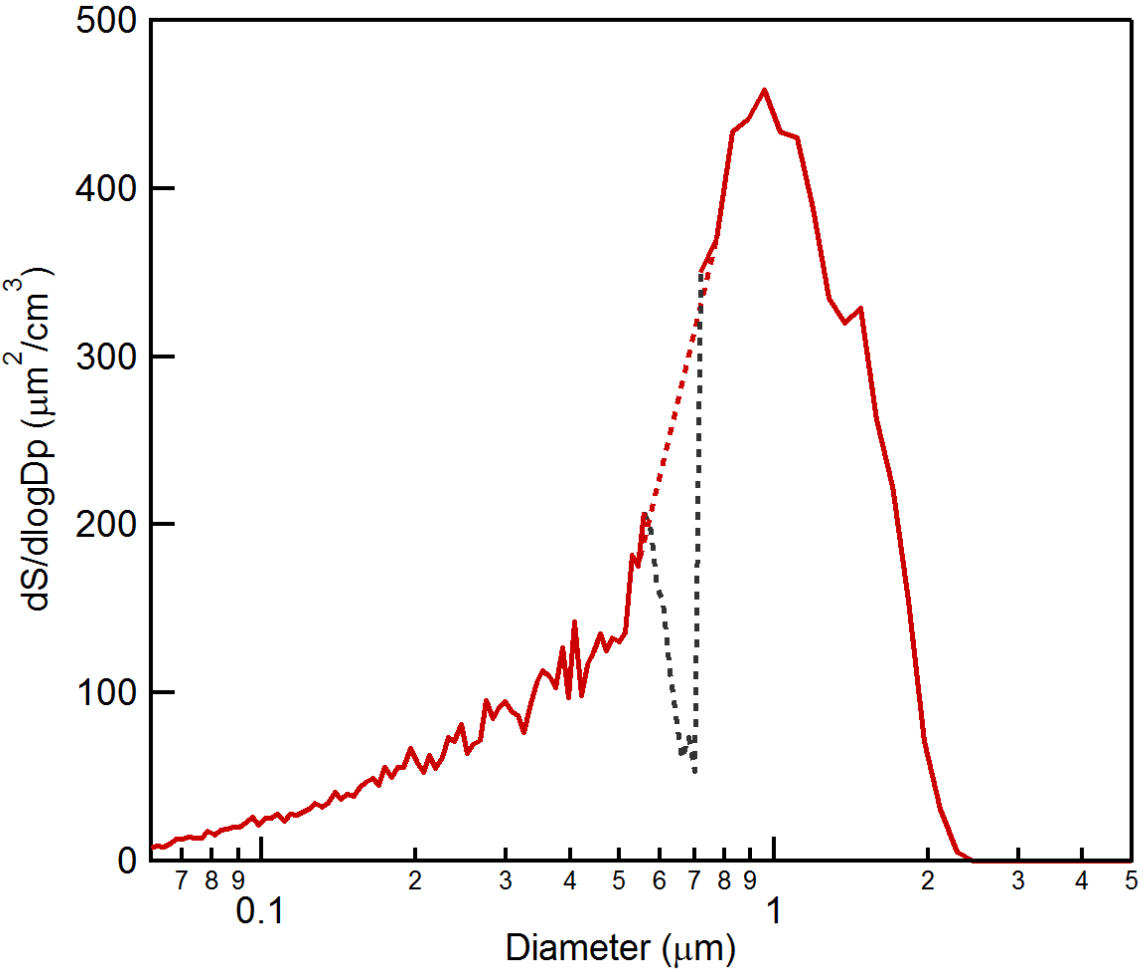

588

589 **Figure 1:** Representative surface area distribution for SSA produced in the MART system after applying
590 a growth factor value of 2.3, and adjusting for dilution of the SSA concentration to the sizing
591 instrumentation so as not to saturate the detectors. The black dotted line results from combining UHSAS
592 and APS surface area distributions, and the red dotted line is the data interpolation used over this region.

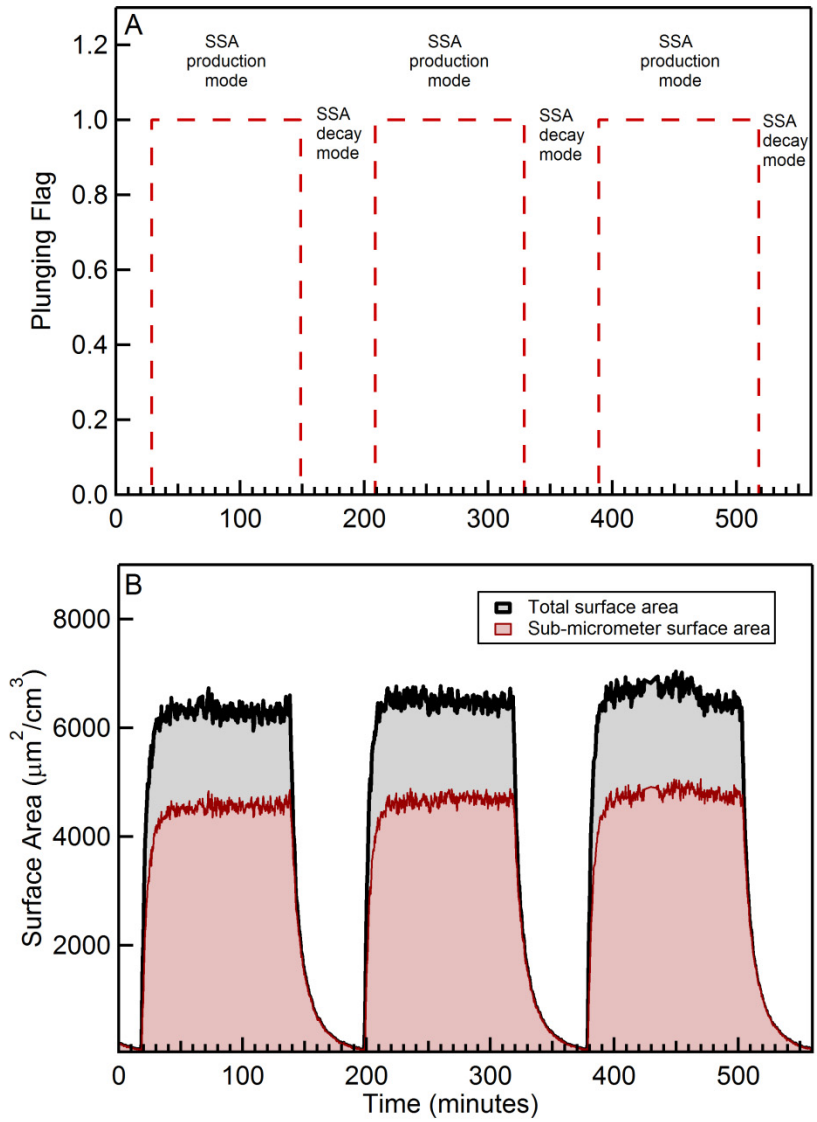

Figure 2: Plunging duty cycle flag as a function of time (Panel A) where a value of 1 indicates plunging is turned on for SSA production mode, and a value of zero indicates plunging is turned off. Panel B shows the response of the total (black) and sub-micrometer (red) surface area to changes in the plunging duty cycle as a function of time.

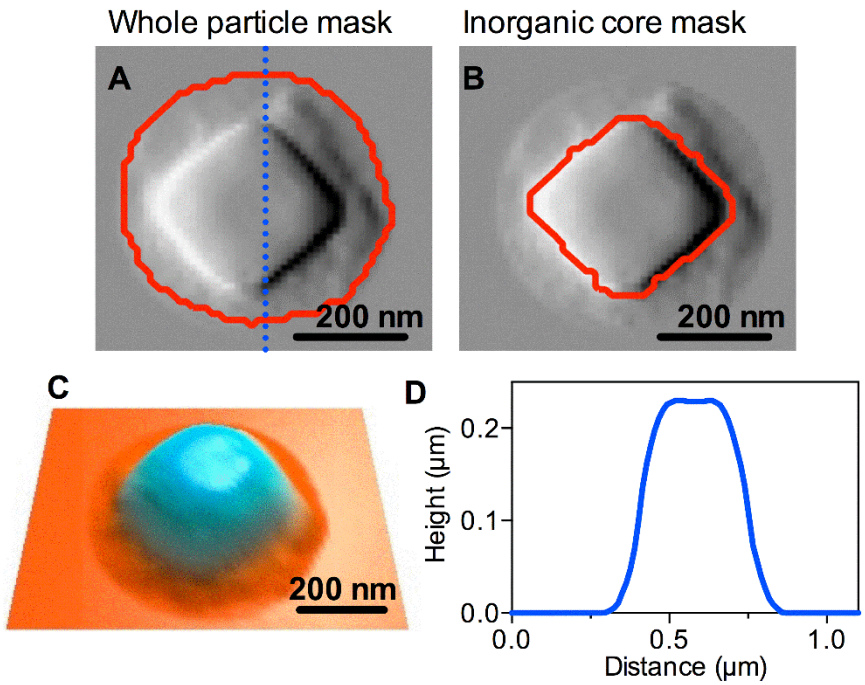

599
600

601 **Figure 3**: AFM amplitude (A, B) and 3-dimensional height (C) images taken at ~20-21 % RH, of a sea
602 spray particle generated in the MART, post-galactose addition showing the whole particle mask (Panel
603 A), and the inorganic core mask (Panel B) used to determine upper limit organic volume fractions of
604 imaged particles. Panel D shows cross sectional profile, corresponding to the blue dashed line in A.

605

606

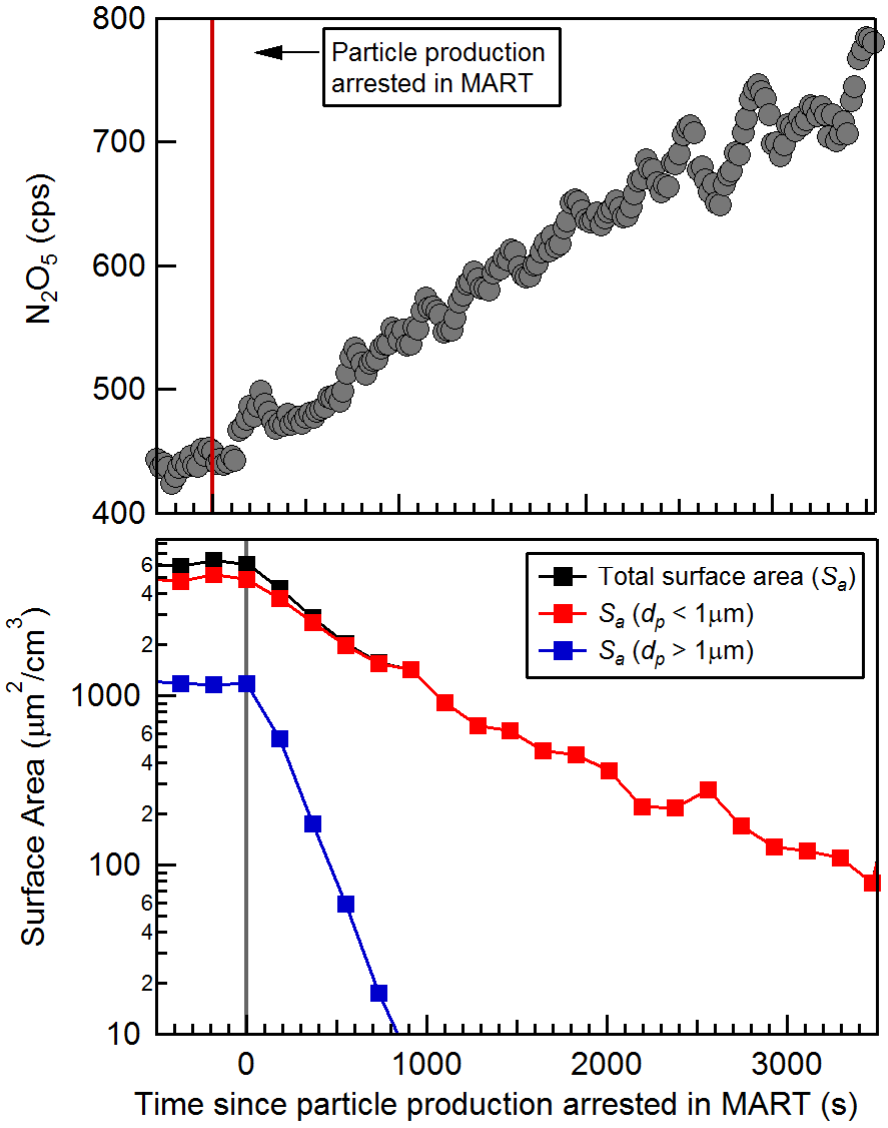

607

608 **Figure 4**: Panel A illustrates the N_2O_5 signal following plunging turning off. Panel B shows a
609 representative time trace of total particle surface area (black), super-micrometer surface area (blue), and
610 sub-micrometer surface area (red) during a typical experimental cycle, where time = 0 corresponds to
611 plunging turned off, thus switching from SSA production mode to SSA decay mode. The vertical red line
612 (Panel A) and grey line (Panel B) indicate the point at which plunging was turned off.

613

614

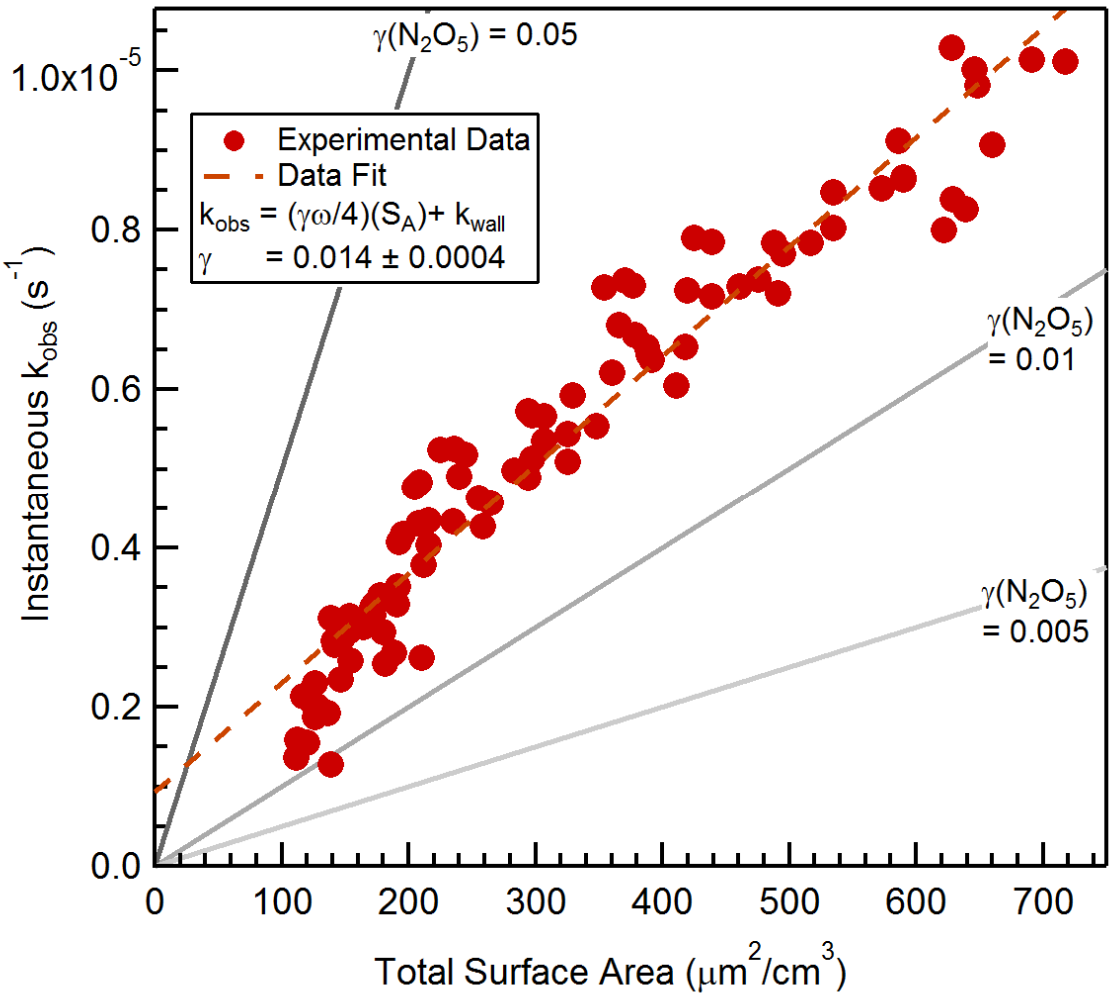

615

616 **Figure 5**: Representative plot of instantaneous k_{obs} versus the total surface area in the flow reactor. Data
617 was filtered such that over the length of one period of residence time in the flow reactor, the surface area
618 was not changing by more than 20 % (see text for details).

619

620

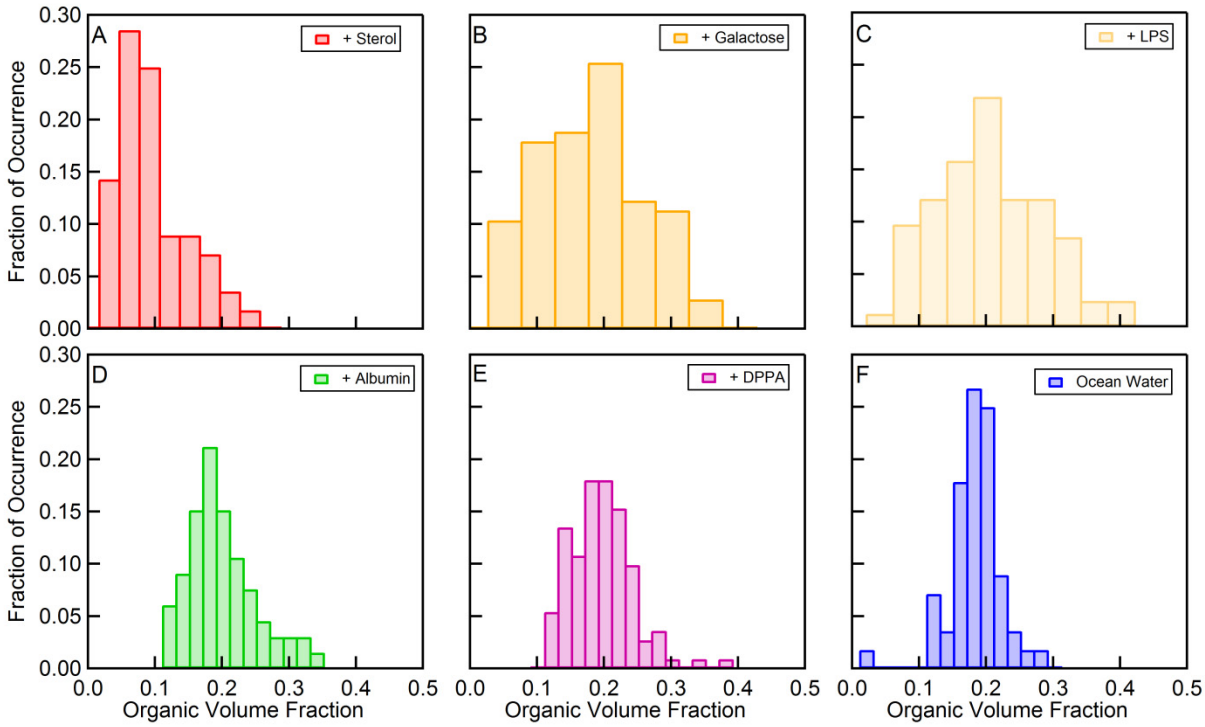

621

622 **Figure 6**: AFM derived organic volume fraction of 0.33-0.56 µm particles (measured as diameter = 0.21
623 µm at 20 % RH by AFM) collected using a MOUDI, imaged for each water matrix vs. the fraction of
624 occurrence.

625

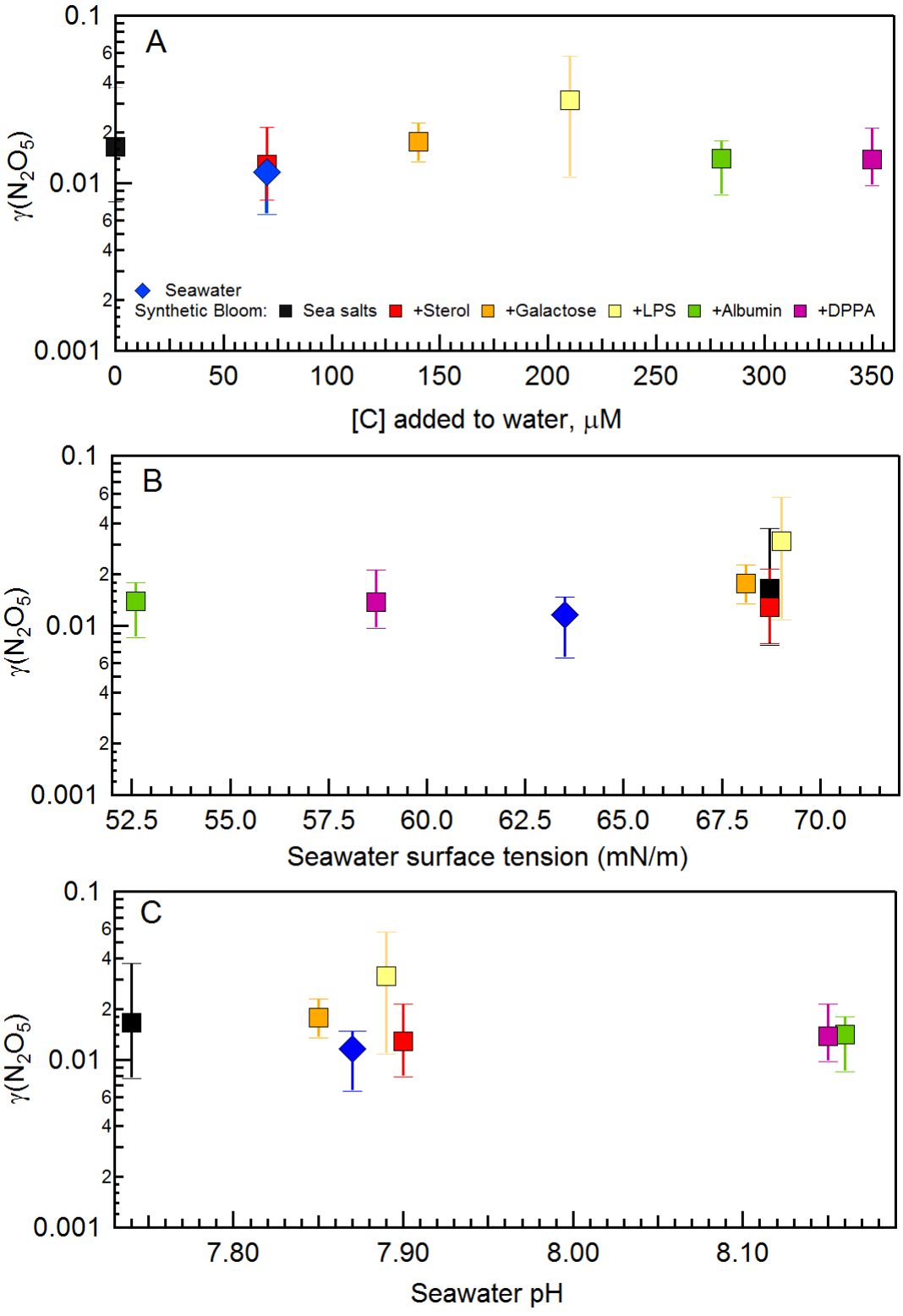
A
B
C
$\gamma(N_2O_5)$
0.1
0.01
0.001
Seawater
Synthetic Bloom:
Sea salts
+Sterol
+Galactose
+LPS
+Albumin
+DPPA
0
50
100
150
200
250
300
350
[C] added to water, μM
52.5
55.0
57.5
60.0
62.5
65.0
67.5
70.0
Seawater surface tension (mN/m)
7.80
7.90
8.00
8.10
Seawater pH

626

Figure 7: Observed dependence of $\gamma(N_2O_5)$ on various seawater properties including carbon concentration added to the water matrix (A), surface tension (B), water pH (C). Data from the synthetic bloom experiment are shown with colored squares and data from the experiment using natural seawater is shown in blue diamonds.

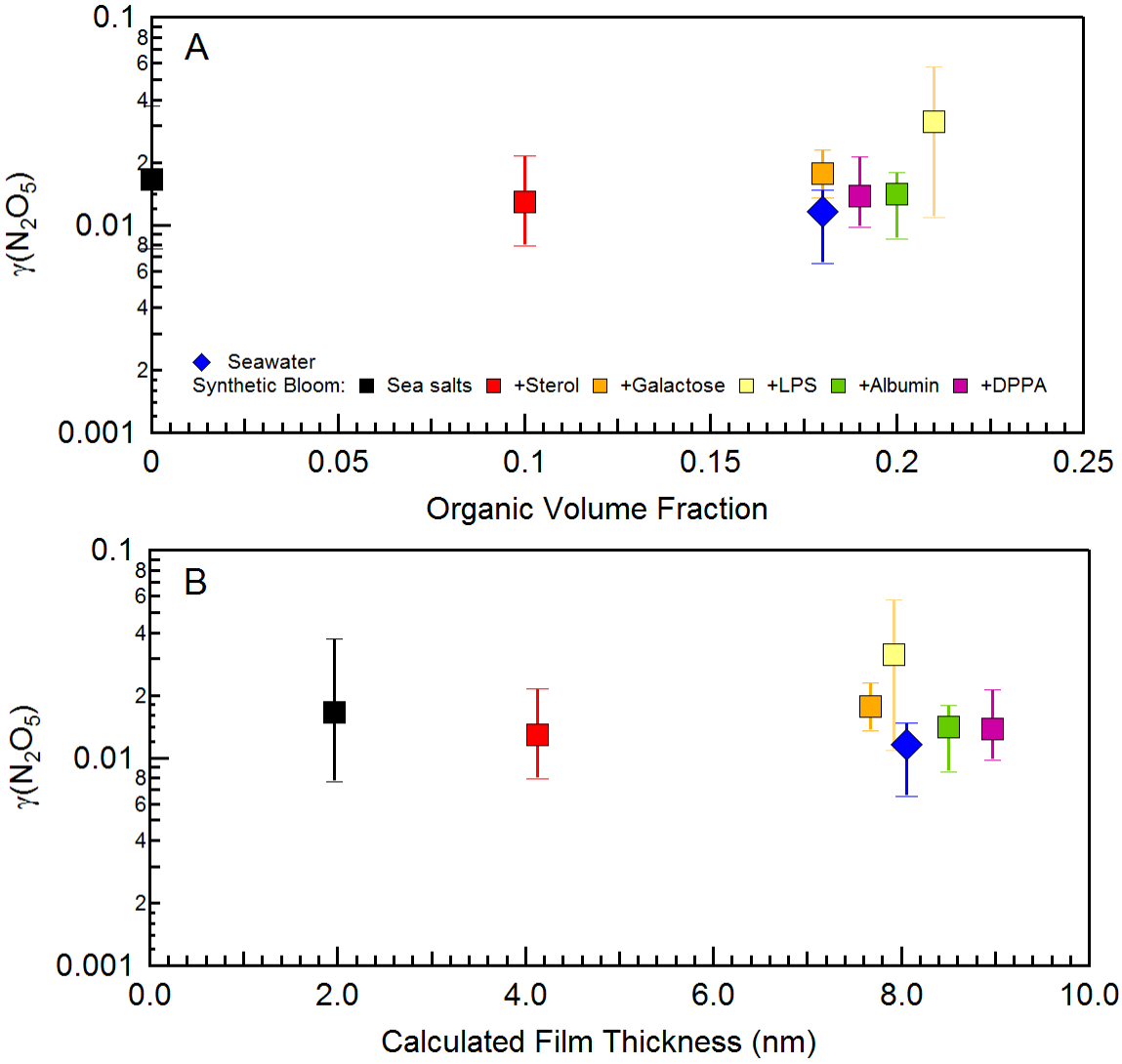

Figure 8: Observed dependence of $\gamma(N_2O_5)$, measured between 50-65% RH, on the derived organic aerosol volume fraction (A) and organic film thickness (B) determined using AFM at 20% RH. Data from the synthetic bloom experiment are shown with colored squares and data from the experiment using natural seawater is shown in blue diamonds.

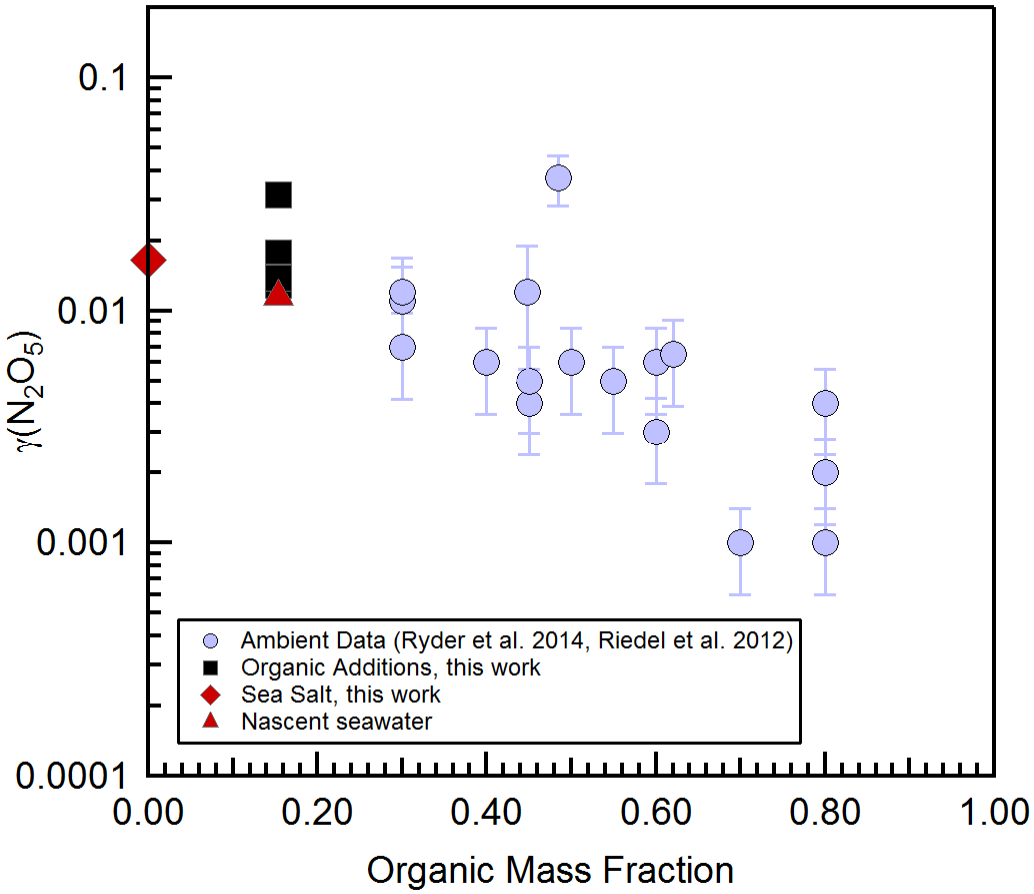

Figure 9. $\gamma(N_2O_5)$ for salt water (red diamond) and following organic additions from this work (black squares) as compared to values obtained from nascent sea-water collected from the SIO pier (red triangle), and ambient data taken from a coastal environment (blue).[20,34]